C-terminal peptides coassemble into Aβ42 oligomers and protect neurons against Aβ42-induced neurotoxicity

Erica A. Fradinger*†, Bernhard H. Monien*‡, Brigita Urbanc§¶, Aleksey Lomakin‖, Miao Tan**, Huiyuan Li*, Sean M. Spring*, Margaret M. Condron*, Luis Cruz§¶, Cui-Wei Xie**††, George B. Benedek‖‡‡§§, and Gal Bitan*††§§¶¶

Departments of *Neurology and **Psychiatry and Biobehavioral Sciences, David Geffen School of Medicine, ††Brain Research Institute, and ¶¶Molecular Biology Institute, University of California, Los Angeles, CA 90095; §Center for Polymer Studies, Department of Physics, Boston University, Boston, MA 02215; and ‖Center for Material Science and Engineering, Material Processing Center, and ‡‡Department of Physics, Massachusetts Institute of Technology, Cambridge, MA 02139

Alzheimer's disease (AD) is an age-related disorder that threatens to become an epidemic as the world population ages. Neurotoxic oligomers of Aβ42 are believed to be the main cause of AD; therefore, disruption of Aβ oligomerization is a promising approach for developing therapeutics for AD. Formation of Aβ42 oligomers is mediated by intermolecular interactions in which the C terminus plays a central role. We hypothesized that peptides derived from the C terminus of Aβ42 may get incorporated into oligomers of Aβ42, disrupt their structure, and thereby inhibit their toxicity. We tested this hypothesis using Aβ fragments with the general formula Aβ(x–42) (x = 28–39). A cell viability screen identified Aβ(31–42) as the most potent inhibitor. In addition, the shortest peptide, Aβ(39–42), also had high activity. Both Aβ(31–42) and Aβ(39–42) inhibited Aβ-induced cell death and rescued disruption of synaptic activity by Aβ42 oligomers at micromolar concentrations. Biophysical characterization indicated that the action of these peptides likely involved stabilization of Aβ42 in nontoxic oligomers. Computer simulations suggested a mechanism by which the fragments coassembled with Aβ42 to form heterooligomers. Thus, Aβ(31–42) and Aβ(39–42) are leads for obtaining mechanism-based drugs for treatment of AD using a systematic structure–activity approach.

Alzheimer's disease | amyloid β-protein | inhibitor design

Alzheimer's disease (AD) is the predominant cause of dementia and one of the leading causes of death among elderly people. It is estimated that there are currently ≈27 million people suffering from AD worldwide (1). Because the world population is aging rapidly, if no cure is found in the near future AD will become an epidemic (2).

The amyloid cascade hypothesis proposed that amyloid β-protein (Aβ) fibrils—an aggregated form of Aβ found in amyloid plaques in the brains of patients with AD—were the neurotoxic agents causing AD (3). However, in recent years, multiple lines of evidence have led to a revision of this view, and today the primary toxins causing AD are believed to be early-forming Aβ oligomers rather than Aβ fibrils (4, 5). This paradigm shift suggests that efforts toward development of therapeutic agents targeting Aβ assembly should be directed at Aβ oligomers rather than fibrils. In particular, genetic, physiologic, and biochemical data indicate that oligomers of the 42-aa form of Aβ, Aβ42, are most strongly linked to the etiology of AD (6–9) and therefore are a particularly attractive target for inhibitor design.

Several groups have reported small-molecule inhibitors of Aβ oligomerization (10–13). The importance of understanding the mechanism of inhibition recently has been highlighted (14) after findings that many small-molecule inhibitors of fibrillogenesis may act nonspecifically, likely making them unsuitable for treating amyloid-related disorders (15). In addition, inhibition of fibril formation may actually lead to stabilization of toxic

oligomers (16). Interestingly, when oligomers are stabilized by interaction with inhibitors or modulators, the toxicity of the resulting oligomers depends on the stabilizing molecule. For example, certain inositol derivatives, which were reported to inhibit Aβ-induced toxicity (17), presumably stabilize nontoxic Aβ oligomers (18). Nonetheless, to date, Aβ oligomerization inhibitors have been found empirically with limited mechanistic understanding of how they work, and currently mechanism-based inhibitor design targeting Aβ oligomerization is lacking.

A substantial body of work suggests that the C terminus of Aβ42 is a key region controlling Aβ42 oligomerization. Several studies of prefibrillar Aβ have suggested that the C terminus of Aβ42 is more rigid than the C terminus of the more abundant and less toxic Aβ40 (19–22). The increased rigidity has been attributed to interactions involving the C-terminal residues I41–A42, which stabilize a putative turn conformation (23). The higher conformational stability in the C terminus of Aβ42 correlates with formation oligomer populations distinct from those of Aβ40 (8, 23, 24) and with higher neurotoxicity (7, 9). Based on these data we hypothesized that molecules that possess high affinity for the C terminus of Aβ42 may disrupt oligomer formation and inhibit Aβ42-induced neurotoxicity. Because homotypic intermolecular interactions in the C terminus appear to be particularly important for Aβ42 self-assembly, we reasoned that peptides derived from this region might act as such inhibitors [supporting information (SI) Fig. S1]. We therefore prepared a series of Aβ42 C-terminal fragments (CTFs) (Table 1) and tested their capability of inhibiting Aβ42 toxicity and oligomerization.

Results

Solubility of CTFs. Being highly hydrophobic peptides, the CTFs were expected to be poorly soluble and to aggregate in aqueous solutions. To assess CTF solubility, peptide solutions were

NEUROSCIENCE

Table 1. Sequence and solubility of CTFs used in this study

| CTF	Sequence	Solubility, μM
Aβ(28–42)	KGAIIGLMVGGVVIA	$\approx$1
Aβ(29–42)	GAIIGLMVGGVVIA	22 ± 9
Aβ(30–42)	AIIGLMVGGVVIA	11 ± 3
Aβ(31–42)	IIGLMVGGVVIA	62 ± 18
Aβ(32–42)	IGLMVGGVVIA	52 ± 24
Aβ(33–42)	GLMVGGVVIA	134 ± 37
Aβ(34–42)	LMVGGVVIA	132 ± 29
Aβ(35–42)	MVGGVVIA	149 ± 33
Aβ(36–42)	VGGVVIA	134 ± 20
Aβ(37–42)	GGVVIA	143 ± 27
Aβ(38–42)	GVVIA	156 ± 33
Aβ(39–42)	VVIA	141 ± 30

The solubility values are average concentrations (±SE) measured by AAA for filtered solutions of each CTF in four to seven independent experiments.

prepared by initial dissolution in dilute NaOH (25), followed by dilution in phosphate buffer at physiologic pH and filtration through 20-nm cutoff filters. The concentration of each sample was then measured by amino acid analysis (AAA) (Table 1). CTFs up to 10 aa long could be dissolved at concentrations between 100 and 200 μM. Longer peptides had low solubility, but, except for Aβ(28–42), the solubility was sufficient for evaluation of neurotoxicity inhibition. Measurement of particle size by dynamic light scattering (DLS), β-sheet content by CD spectroscopy, and peptide morphology by EM indicated that, upon incubation in aqueous buffer at pH 7.4, CTFs longer than 5 aa aggregated at rates that ranged from a few hours to a few days depending on peptide length and sequence (data not shown). Direct comparison of aggregation rates was difficult because of the different solubility of the peptides.

Evaluation of CTF Toxicity. As peptides derived from Aβ42, the CTFs may have been neurotoxic themselves. To test for self-toxicity, CTFs were solubilized initially in DMSO and then diluted in cell culture medium. The solution was then centrifuged for 5 min at 16,000 × g to remove preformed large aggregates. The supernatant was added to differentiated PC-12 cells at the desired concentration. All of the solutions were clear to the eye when added to the cells, and the media remained clear at the end of the incubation period. Most of the CTFs showed no toxicity to neuronal cells up to the highest concentration used as assessed by the 3-(4,5-dimethylthiazol-2-yl)-2,5-diphenyltetrazolium bromide (MTT) cell-metabolism assay (26) (Fig. 1A), suggesting that they could be tested for inhibition of Aβ42-induced toxicity. An exception was Aβ(28–42), which was highly toxic (Fig. 1A), possibly because of the presence of K at the N terminus, which increases the positive charge at physiologic pH relative to the other CTFs.

Screening of CTFs for Inhibitory Activity. To evaluate the CTFs for inhibition of Aβ42-induced neurotoxicity, Aβ42 was dissolved in DMSO and diluted into cell culture medium. CTFs then were dissolved in DMSO and mixed with Aβ42 at an Aβ42:CTF concentration ratio of 1:10, respectively. The solution was centrifuged for 5 min at 16,000 × g to remove preformed aggregates and then added to differentiated PC-12 cells and incubated for 15 h. Cell viability was assessed by using the MTT assay.

All 12 CTFs were found to protect the cells to some degree from Aβ42-induced toxicity (Fig. 1B). Among them, Aβ(31–42) showed the highest inhibitory activity, fully rescuing the cells from Aβ42-induced toxicity. Aβ(39–42), the shortest CTFs used (only four amino acid residues), also showed high inhibitory activity (Fig. 1B). We therefore focus further discussion on these
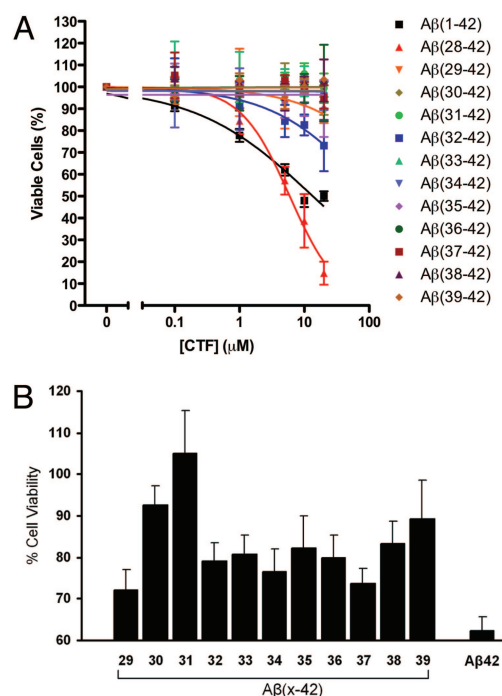

Fig. 1. Evaluation of CTF effect on neuronal cultures. CTFs at final nominal concentrations of 0.1–20 μM or mixtures of Aβ42:CTF at a 1:10 concentration ratio, respectively, were incubated with differentiated PC-12 cells. In A, Aβ42 (black squares) is shown for comparison. In B, the nominal concentration of Aβ42 is 5 μM. After 15 h of incubation, cell viability was measured by using the MTT assay. Cell culture medium containing DMSO in the same concentrations as used for peptide solubilization was used as a negative control, and 1 μM staurosporine was used as a positive control. The graphs show average data ± SD from at least three independent experiments, each performed with six wells per condition.

two peptides. Although Aβ(30–42) showed an activity level similar to that of Aβ(39–42), it was a less interesting peptide to study because it is structurally similar to, but less active than, Aβ(31–42).

Further Evaluation of Aβ(31–42) and Aβ(39–42) as Inhibitors of Aβ-Induced Neurotoxicity. To study the effectiveness of Aβ(31–42) and Aβ(39–42) as inhibitors of Aβ42-induced toxicity, dose dependence curves were generated. Aβ(31–42) and Aβ(39–42) yielded IC$_{50}$ values of 14 ± 2 and 16 ± 5 μM in the MTT assay (Fig. S2A). The MTT assay measures cell metabolism rather than cell viability *per se*; however, because of the relatively short period required for this assay, it is a standard assay for investigations of Aβ toxicity (26, 27). In addition, Aβ(31–42) and Aβ(39–42) yielded IC$_{50}$ values of 20 ± 4 and 47 ± 14 μM, respectively, in the lactate dehydrogenase (LDH) release assay (Fig. S2B), a direct measurement of cell death (28).

Synaptic failure has been postulated to be the primary event leading to the development of AD (5, 29). A decrease in the frequency of spontaneous miniature excitatory postsynaptic currents (mEPSCs) reflects a decline in the number of functional excitatory synapses or a reduction in presynaptic release probability. Aβ has been shown to inhibit synaptic function and decrease mEPSC frequency (30, 31). Here we used Aβ-induced attenuation of mEPSC frequency in primary mouse hippocampal neurons to evaluate the ability of Aβ(31–42) and Aβ(39–42) to rescue Aβ42-mediated synaptic toxicity.

Aβ42 and CTF mixtures were prepared in a manner similar to that used for cell viability assays, except that perfusion buffer (vehicle) was used instead of cell culture medium. After estab-
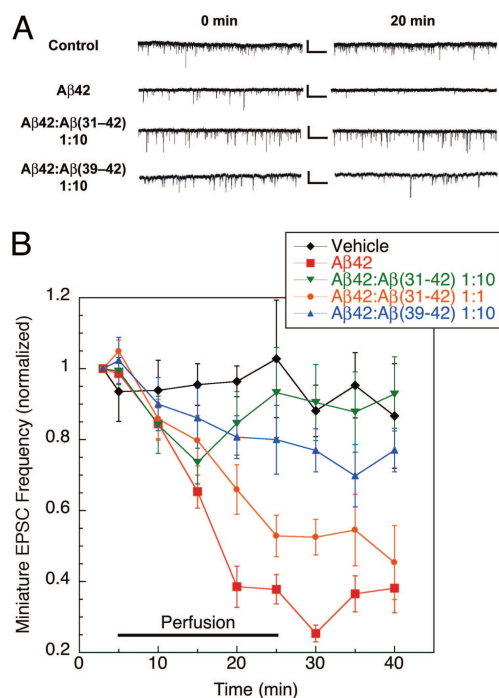
Fig. 2. CTFs rescue mEPSCs in Aβ42-treated hippocampal neurons. Mouse primary hippocampal neurons were exposed to vehicle (*n* = 5), 3 μM Aβ42 (*n* = 8), 1:1 Aβ42:Aβ(31–42) (*n* = 9), 1:10 Aβ42:Aβ(31–42) (*n* = 10), or 1:10 Aβ42:Aβ(39–42) (*n* = 6) mixtures, and the frequency and amplitude of mEPSCs were measured. (*A*) Representative recording traces collected before (0 min) and 20 min after peptide perfusion. Calibration bars: 25 pA/1 sec. (*B*) Cells were perfused with vehicle for 5 min to establish baseline, and then with peptide solutions for an additional 20 min, and allowed to recover in vehicle solution for 15 min. The curves show the time dependence of mEPSC frequency after exposure to Aβ42 in the absence or presence of CTFs over 40 min.

lishing a stable baseline recording for 5 min, cells were perfused with vehicle, Aβ42, or Aβ42:CTF mixtures at either 1:10 (both CTFs) or 1:1 [Aβ(31–42) only] concentration ratios, respectively, for 20 min, and washed for 15 min after perfusion. At 3 μM, Aβ42 was found to induce robust inhibition of mEPSCs, reducing spike frequency by 60–70% relative to baseline levels within 20 min (Fig. 2). This effect persisted after a 15-min washing period. Significant inhibition of the toxic effect of Aβ42 was observed at a 1:1 Aβ42:Aβ(31–42) concentration ratio, and at 10-fold excess Aβ(31–42) rescued mEPSC deficits completely (Fig. 2*B*), demonstrating that the CTF not only protected neuron viability, but also protected synaptic function from toxic insults by Aβ42 oligomers. Aβ(39–42) showed a somewhat lower, yet significant (*P* < 0.05), inhibitory effect at 10-fold excess relative to Aβ42 and was not studied at lower concentration ratios (Fig. 2). Changes in the amplitude of mEPSCs in the presence of Aβ42 or Aβ42:CTF mixtures relative to vehicle were not significant.

CTF Effect on Aβ42 Assembly. To gain insight into the mechanism by which CTFs inhibit Aβ42-induced toxicity we studied the interaction between the CTFs and Aβ42 during assembly using DLS, photo-induced cross-linking of unmodified proteins (PICUP), and discrete molecular dynamics (DMD), methods that have been useful for study of Aβ assembly (32–34).

For DLS experiments, mixtures of Aβ42:CTF at 30 μM nominal concentration each were prepared in 10 mM sodium phosphate (pH 7.4) and compared with Aβ42 alone. The actual concentration was determined *post facto* for each experiment by AAA. In the absence of CTFs, Aβ42 comprised predominantly particles with a hydrodynamic radius R_{H1} of ≈8–12 nm, which we

designated as population 1 (P1, Fig. 3*A*, white bars). A minor population of larger particles, P2, with R_{H2} ≈ 20–60 nm was observed in some, but not all, measurements. Both Aβ(31–42) and Aβ(39–42) induced substantial formation and accumulation of P2 particles (Fig. 3*A Top* and *Middle*, gray bars). In addition, Aβ(39–42) caused compaction of P1 particles to R_{H1} of ≈4–9 nm, whereas Aβ(31–42) did not. After 7 days of incubation in the absence of CTFs, Aβ42 formed particles of R_H ≈ 500–1,000 nm (Fig. 3*A Bottom*, gray bars). Over a similar time period, slow growth of P2 up to an R_{H2} of ≈300 nm was observed in Aβ42:CTF mixtures. Quantitative analysis showed that the growth rate of P2 particles, dR_{H2}/dt, was decreased substantially in the presence of both CTFs relative to Aβ42 alone (Fig. 3*B*). It is important to note that, even though CTFs increase the abundance of P2 oligomers, the fraction of these oligomers is overrepresented in the DLS experiments because scattering from large particles is magnified proportionally to the square of their mass. Thus, P2 assemblies account for no more than a few percent of the total Aβ population.

In control DLS experiments using CTFs in the absence of full-length Aβ42 we observed a behavior different from the one described above. At 50 μM, Aβ(31–42) aggregated slowly, reaching particle size of ≈100 nm after several days. Distinct oligomer populations similar to P1 or P2 were not observed. Aβ(39–42) showed no aggregation at concentrations up to 140 μM.

As a complementary method for evaluating aggregation in Aβ42:CTF mixtures, we measured the average frequency of intensity spikes that occur when large particles, presumably fibrils, cross the DLS instrument's laser beam during the first 3 days of incubation (Fig. 3*C*). Both Aβ(31–42) and Aβ(39–42) showed substantial inhibition of fibril growth relative to Aβ42.

Next we investigated the effect of CTFs on formation of small oligomers using PICUP. When low-molecular-weight (LMW) Aβ42 (35) is subjected to PICUP and analyzed by SDS/PAGE, the most abundant oligomers observed are pentamers and hexamers, which self-assemble to form larger oligomers and therefore have been termed paranuclei (8). Paranucleus formation requires no incubation—these oligomers are observed immediately after dissolution and cross-linking of Aβ42. To study the effect of CTFs on these early-forming Aβ oligomers, ≈30 μM LMW Aβ42 was mixed with CTFs and cross-linked immediately. Importantly, the CTFs contain only residues that have little or no reactivity in PICUP chemistry (33). Therefore, cross-linking of CTFs to Aβ42 or to themselves was not observed, facilitating unhindered analysis of Aβ42 oligomer size distributions. Aβ(31–42) was found to cause a dose-dependent decrease in the formation of Aβ42 paranuclei at concentrations between ≈3 and 35 μM (Fig. S3) whereas Aβ(39–42) did not show this effect at a concentration as high as 155 μM (Fig. S3*B*). These data suggest that as the PICUP-inert Aβ(31–42) molecules coassemble with Aβ42, they spatially separate and "dilute" the Aβ42 monomers, preventing cross-linking. Aβ(39–42) might have induced a similar effect at a higher concentration if such high solubility could have been achieved. Alternatively, Aβ(39–42) may interfere with Aβ42-induced toxicity by a distinct mechanism that does not affect cross-linking.

Because of their noncrystalline and metastable nature, Aβ oligomers are not amenable to structural investigation using high-resolution experimental techniques, such as x-ray crystallography or solution-state NMR. To study the interactions between Aβ42 and CTFs during oligomerization in high resolution, we used computer simulations that combine DMD and a simplified protein structure. This approach, unlike traditional molecular dynamics using all-atom models, enables modeling of large molecular ensembles within relatively short times (34). Previously, this modeling strategy was used to study the oli-
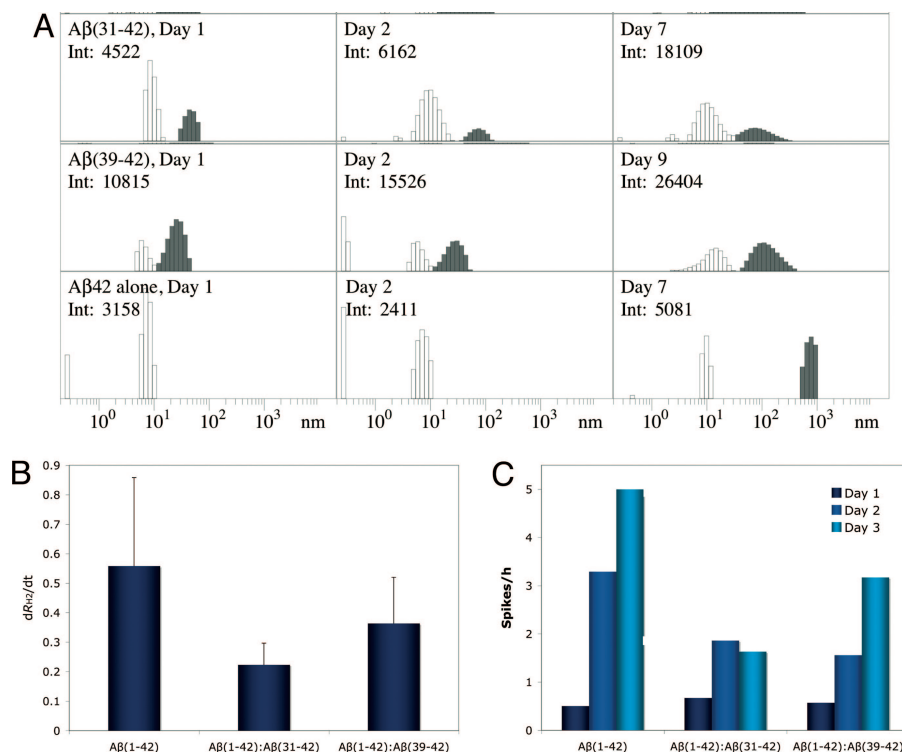
Fig. 3. CTF effect on Aβ42 assembly. (*A*) Representative distributions of Aβ42 in the absence or presence of CTFs immediately after preparation (*Left*), on the next day (*Center*), and after 7 or 9 days (*Right*). White bars represent P1 particles. Gray bars represent P2 or larger particles (in the case of Aβ42 alone). Days of measurement and the total scattering intensities in counts per second are shown in the upper left corner of each panel. Only intensities within the same row are directly comparable with each other. (*B*) Growth rates of P2 particles (dR_{H2}/dt) in the absence or presence of CTFs. (*C*) Average number of intensity spikes per hour during the first 3 days of measurement in the absence or presence of CTFs.

gomerization processes of Aβ40 and Aβ42 (23, 24), yielding oligomer size distributions in good agreement with experimental findings (8, 36).

Here we modeled the self-assembly of Aβ42 in the presence of Aβ(31–42) or Aβ(39–42), each at Aβ42:CTF number concentration ratios ranging from 1:1 to 1:8. In all cases, we found that Aβ42 and the CTF molecules coassembled into "heterooligomers." An example is shown in Fig. 4*A*. Formation of heterooligomers of Aβ42 and Aβ(31–42) was observed already after 10^5 simulation steps, and by 10^7 steps all of the molecules associated into one large heterooligomer. Movie S1 shows the time evolution of the heterooligomers. This behavior was observed for the Aβ42:Aβ(31–42) system at 1:2 and higher ratios, whereas in the Aβ42:Aβ(39–42) system a 1:8 ratio was necessary for the coassembly of all of the molecules into one heterooligomer. Within the heterooligomers, intermolecular interactions among Aβ42 monomers were inhibited. Aβ(31–42) was found to inhibit these intermolecular interactions substantially more efficiently than Aβ(39–42) (Fig. 4*B*).

Discussion

We have used an approach for developing Aβ42 oligomerization inhibitors based on putative homotypic association of peptide sequences in the C terminus of Aβ42. Peptides derived from the C terminus of Aβ42 were found to disrupt the assembly and inhibit the neurotoxicity of Aβ42 oligomers. This proof-of-concept study using Aβ42 CTFs has yielded two lead peptide inhibitors of Aβ42 assembly and neurotoxicity, Aβ(31–42) and Aβ(39–42). The higher inhibitory activity of Aβ(31–42) and Aβ(39–42) relative to other CTFs suggests that the inhibition is specific rather than based on generic hydrophobic association.

In our initial screen, in which Aβ42 was mixed with each CTF at a 1:10 ratio, respectively, Aβ(31–42) was the only CTF that completely rescued the cells from Aβ42-induced toxicity. It was followed by Aβ(30–42) and Aβ(39–42), each of which attenuated Aβ42 toxicity by ≈80% (Fig. 1*B*). When the inhibitory activity is plotted versus CTF length, Aβ(31–42) gives rise to an inhibitory activity peak (Fig. 1*B*). The high activity of Aβ(30–42) was interpreted as resulting from its close similarity to Aβ(31–42). In contrast, the high activity of Aβ(39–42) was surprising given its small size and presumed absence of stable conformation.

In the three biological tests applied, cell death (LDH assay), mitochondrial integrity (MTT assay), and synaptic function (mEPSC assay), Aβ(31–42) consistently showed higher potency as an inhibitor of Aβ42-induced toxicity than Aβ(39–42). Structural studies of Aβ42 have suggested the existence of a quasi-stable conformation in the C terminus (19–22), likely a turn centered at G37–G38 (23, 24, 37). We conjecture that this conformation is important for intermolecular interaction among the C termini of Aβ42 that lead to oligomerization. A similar putative structure in Aβ(31–42) may account, at least partially, for the high inhibitory activity of this peptide. In contrast, Aβ(39–42) is not expected to have a stable conformation. These considerations, and the fact that Aβ(31–42) is three times as long as Aβ(39–42), suggest that the two CTFs may act by different mechanisms.

We anticipated that CTFs would disrupt Aβ42 oligomerization by incorporating into a putative hydrophobic core of Aβ42 oligomers (Fig. S1), in which the C terminus was predicted to be an important component. Our physicochemical studies suggest that the CTFs indeed interact with Aβ42 molecules and get incorporated into oligomers. DLS data (Fig. 3*A*) show two initial oligomeric populations of Aβ42, high-abundance, small oli-

Fradinger *et al.*
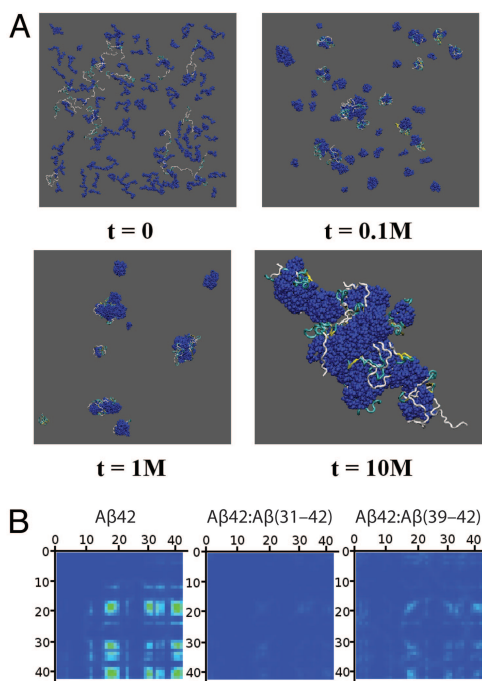
Fig. 4. Simulation of the interaction between Aβ42 and CTFs during oligomerization. (*A*) Configurations of 16 Aβ42 and 128 Aβ(31–42) molecules at different time frames measured at *t* simulation steps. CTFs are displayed in dark blue, and Aβ42 molecules are represented by their secondary structure: yellow ribbons, β-strands; blue tubes, turns; silver tubes, random coil. (*B*) Intermolecular contact maps of Aβ42 in the absence or presence of CTFs calculated for the highest Aβ42:CTF peptide number concentration ratio (1:8). The contact maps are oriented such that the contact strength between pairs of N-terminal residues is displayed at the top left corner and the contact strength between pairs of C-terminal residues is at the bottom right corner. The strength of the contact between two amino acids is color-coded from 0.0 (blue) to a maximal strength (red), corresponding to 30 contacts.

gomers of $R_H \approx 8$–12 nm (P1) and low-abundance, intermediate-size oligomers of $R_H \approx 20$–60 nm (P2). In the presence of Aβ(31–42) and Aβ(39–42), P2 oligomers are stabilized and their growth is attenuated (Fig. 3 *A* and *B*). In addition, both CTFs inhibit formation of intensity spikes in DLS experiments (Fig. 3*C*), suggesting inhibition of fibril formation. In correlation with the higher inhibitory activity observed for Aβ(31–42) in the MTT, LDH, and mEPSC assays, it was found to inhibit both the increase in size of P2 particles and the average number of intensity spikes per hour with higher potency than Aβ(39–42) (Fig. 3 *B* and *C*). In addition, CTFs that showed low inhibition of toxicity had little effect on particle growth (data not shown), demonstrating an overall good agreement between inhibition of particle growth and inhibition of toxicity.

In support of different mechanisms of toxicity inhibition by Aβ(31–42) and Aβ(39–42), only Aβ(39–42) was found to reduce the size of the P1 oligomer population to ≈4–9 nm, suggesting that interaction with Aβ(39–42) altered the tertiary and/or quaternary structure of Aβ42 within P1 oligomers. Another important difference between the two CTFs was found in PICUP experiments, in which Aβ(31–42) was found to inhibit paranucleus formation dose-dependently (Fig. S3), whereas Aβ(39–42) did not show such inhibition at the highest concentration tested (Fig. S3*B*).

The observed differences between the behaviors of Aβ(31–42) and Aβ(39–42) in both the PICUP and the DLS experiments correlated qualitatively with the simulation findings. In agreement with the PICUP data, the model predicted more efficient disruption of intermolecular contacts among Aβ42 monomers by

Aβ(31–42) than by Aβ(39–42) (Fig. 4*B*). The computer simulations also help explaining, qualitatively, how CTFs can both disrupt paranucleus formation and promote formation of P2 oligomers. In the model, relatively large heterooligomers are observed at high numbers of simulation steps (Fig. 4*A*). Interruption of intermolecular contacts within these heterooligomers by CTFs suggests that their cross-linking by PICUP would be inhibited because the cross-linking is "zero length"; i.e., it requires direct intermolecular interactions between Aβ42 monomers.

Taken together, the data indicate that the CTFs inhibit Aβ42-induced toxicity by formation of nontoxic heterooligomers, similar to the mechanism proposed for the inhibitory activity of inositols (17, 18) and for the green tea-derived polyphenol epigallocatechin gallate (38). The observation that highly hydrophobic peptides are acting by a mechanism similar to that of polyols is interesting and suggests that stabilization of nontoxic oligomers may be a general mechanism for compounds that inhibit the toxic effects of amyloidogenic proteins. Using peptides derived from the C terminus of Aβ42, rather than carbohydrate-based inhibitors, allows delineating the relationship between inhibitor structure and bioactivity, providing a framework for development of future derivatives. An advantage of using CTFs as inhibitors is that the hydrophobic nature of these peptides may facilitate penetration through biological barriers, such as the plasma membrane and the blood–brain barrier. Our findings provide a foundation for lead optimization by systematic structure–activity relationship studies. Aβ(31–42) is a potent inhibitor of toxicity that may be optimized by using standard methods, such as alanine scanning and introduction on nonnatural amino acids. Aβ(39–42) is a somewhat weaker inhibitor, but its small size may facilitate transformation into peptidomimetics leading to novel, disease-modifying drugs for AD.

Methods

Peptide Preparation. Aβ42 and CTFs were synthesized by Fmoc chemistry using automated Applied Biosystems 433A synthesizers, purified, and characterized by AAA and mass spectrometry as described previously (39, 40). For additional details, see *SI Text*.

Cell Culture. Rat pheochromocytoma (PC-12) cells were used 48 h after differentiation. Primary embryonic hippocampal cultures were maintained for 2 weeks before initiation of experiments. For additional details, see *SI Text*.

Cell Viability Assays. The biological activity of the CTFs themselves and of Aβ42:CTF mixtures was assessed by the CellTiter 96 Cell Proliferation Assay (MTT assay; Promega) and CytoTox-ONE Homogenous Membrane Integrity Assay (LDH assay; Promega). For additional details, see *SI Text*.

Electrophysiological Studies. Spontaneous mEPSCs were recorded at a holding potential of −70 mV by using an Axopatch 200A patch-clamp amplifier (Axon Instruments). For additional details, see *SI Text*.

DLS. Aβ42:CTF mixtures prepared at 30 μM (nominal concentration) of each peptide were studied by using an in-house-built system with a He-Ne laser model 127 (wavelength 633 nm, power 50 mW; Coherent) as a light source. For additional details, see *SI Text*.

PICUP. Aβ42:CTF mixtures were prepared in 10 mM sodium phosphate (pH 7.4) and subjected immediately to PICUP as described previously (33). For additional details, see *SI Text*.

DMD. DMD simulations were performed by using a four-bead protein model with backbone hydrogen bonding and effective amino acid-specific interactions due to hydropathy, as described previously (23, 24). For additional details, see *SI Text*.

NEUROSCIENCE

1. Brookmeyer R, Johnson E, Ziegler-Graham K, Arrighi HM (2007) Forecasting the global burden of Alzheimer's disease. *Alzheimer's Dementia* 3:186–191.
2. Alzheimer Association (2008) 2008 Alzheimer's disease facts and figures. *Alzheimer's Dementia* 4:110–133.
3. Hardy JA, Higgins GA (1992) Alzheimer's disease: The amyloid cascade hypothesis. *Science* 256:184–185.
4. Kirkitadze MD, Bitan G, Teplow DB (2002) Paradigm shifts in Alzheimer's disease and other neurodegenerative disorders: The emerging role of oligomeric assemblies. *J Neurosci Res* 69:567–577.
5. Walsh DM, Selkoe DJ (2007) Aβ oligomers—A decade of discovery. *J Neurochem* 101:1172–1184.
6. Borchelt DR, *et al.* (1996) Familial Alzheimer's disease-linked presenilin 1 variants elevate Aβ1–42/1–40 ratio in vitro and in vivo. *Neuron* 17:1005–1013.
7. Dahlgren KN, *et al.* (2002) Oligomeric and fibrillar species of amyloid-β peptides differentially affect neuronal viability. *J Biol Chem* 277:32046–32053.
8. Bitan G, *et al.* (2003) Amyloid β-protein (Aβ) assembly: Aβ40 and Aβ42 oligomerize through distinct pathways. *Proc Natl Acad Sci USA* 100:330–335.
9. McGowan E, *et al.* (2005) Aβ42 is essential for parenchymal and vascular amyloid deposition in mice. *Neuron* 47:191–199.
10. Wang Z, Chang L, Klein WL, Thatcher GR, Venton DL (2004) Per-6-substituted-per-6-deoxy β-cyclodextrins inhibit the formation of β-amyloid peptide derived soluble oligomers. *J Med Chem* 47:3329–3333.
11. Walsh DM, *et al.* (2005) Certain inhibitors of synthetic amyloid β-peptide (Aβ) fibrillogenesis block oligomerization of natural Aβ and thereby rescue long-term potentiation. *J Neurosci* 25:2455–2462.
12. Yang F, *et al.* (2005) Curcumin inhibits formation of amyloid β oligomers and fibrils, binds plaques, and reduces amyloid in vivo. *J Biol Chem* 280:5892–5901.
13. Necula M, Kayed R, Milton S, Glabe CG (2007) Small molecule inhibitors of aggregation indicate that amyloid β oligomerization and fibrillization pathways are independent and distinct. *J Biol Chem* 282:10311–10324.
14. Research Highlights (2008) Chemical biology: Aggravating aggregating. *Nature* 451:608–609.
15. Feng BY, *et al.* (2008) Small-molecule aggregates inhibit amyloid polymerization. *Nat Chem Biol* 4:197–199.
16. Martins IC, *et al.* (2008) Lipids revert inert Aβ amyloid fibrils to neurotoxic protofibrils that affect learning in mice. *EMBO J* 27:224–233.
17. McLaurin J, *et al.* (2006) Cyclohexanehexol inhibitors of Aβ aggregation prevent and reverse Alzheimer phenotype in a mouse model. *Nat Med* 12:801–808.
18. McLaurin J, Golomb R, Jurewicz A, Antel JP, Fraser PE (2000) Inositol stereoisomers stabilize an oligomeric aggregate of Alzheimer amyloid β peptide and inhibit Aβ-induced toxicity. *J Biol Chem* 275:18495–18502.
19. Murakami K, *et al.* (2005) Formation and stabilization model of the 42-mer Aβ radical: Implications for the long-lasting oxidative stress in Alzheimer's disease. *J Am Chem Soc* 127:15168–15174.
20. Riek R, Guntert P, Döbeli H, Wipf B, Wüthrich K (2001) NMR studies in aqueous solution fail to identify significant conformational differences between the monomeric forms of two Alzheimer peptides with widely different plaque-competence, Aβ(1–40)[ox] and Aβ(1–42)[ox]. *Eur J Biochem* 268:5930–5936.
21. Sgourakis NG, Yan Y, McCallum SA, Wang C, Garcia AE (2007) The Alzheimer's peptides Aβ40 and 42 adopt distinct conformations in water: A combined MD/NMR study. *J Mol Biol* 368:1448–1457.
22. Lazo ND, Grant MA, Condron MC, Rigby AC, Teplow DB (2005) On the nucleation of amyloid β-protein monomer folding. *Protein Sci* 14:1581–1596.
23. Urbanc B, *et al.* (2004) *In silico* study of amyloid β-protein folding and oligomerization. *Proc Natl Acad Sci USA* 101:17345–17350.
24. Yun S, *et al.* (2007) Role of electrostatic interactions in amyloid β-protein (Aβ) oligomer formation: A discrete molecular dynamics study. *Biophys J* 92:4064–4077.
25. Fezoui Y, *et al.* (2000) An improved method of preparing the amyloid β-protein for fibrillogenesis and neurotoxicity experiments. *Amyloid* 7:166–178.
26. Datki Z, *et al.* (2003) Method for measuring neurotoxicity of aggregating polypeptides with the MTT assay on differentiated neuroblastoma cells. *Brain Res Bull* 62:223–229.
27. Shearman MS, Ragan CI, Iversen LL (1994) Inhibition of PC12 cell redox activity is a specific, early indicator of the mechanism of β-amyloid-mediated cell death. *Proc Natl Acad Sci USA* 91:1470–1474.
28. Korzeniewski C, Callewaert DM (1983) An enzyme-release assay for natural cytotoxicity. *J Immunol Methods* 64:313–320.
29. Haass C, Selkoe DJ (2007) Soluble protein oligomers in neurodegeneration: Lessons from the Alzheimer's amyloid β-peptide. *Nat Rev Mol Cell Biol* 8:101–112.
30. Chin JH, Ma L, MacTavish D, Jhamandas JH (2007) Amyloid β protein modulates glutamate-mediated neurotransmission in the rat basal forebrain: Involvement of presynaptic neuronal nicotinic acetylcholine and metabotropic glutamate receptors. *J Neurosci* 27:9262–9269.
31. Parameshwaran K, *et al.* (2007) Amyloid β-peptide Aβ(1–42) but not Aβ(1–40) attenuates synaptic AMPA receptor function. *Synapse* 61:367–374.
32. Lomakin A, Teplow DB (2006) Quasielastic light scattering study of amyloid β-protein fibril formation. *Protein Pept Lett* 13:247–254.
33. Bitan G (2006) Structural study of metastable amyloidogenic protein oligomers by photo-induced cross-linking of unmodified proteins. *Methods Enzymol* 413:217–236.
34. Urbanc B, Borreguero JM, Cruz L, Stanley HE (2006) Ab initio discrete molecular dynamics approach to protein folding and aggregation. *Methods Enzymol* 412:314–338.
35. Bitan G, Teplow DB (2005) Preparation of aggregate-free, low molecular weight amyloid-β for assembly and toxicity assays. *Methods Mol Biol* 299:3–9.
36. Bernstein SL, *et al.* (2005) Amyloid β-protein: Monomer structure and early aggregation states of Aβ42 and its Pro19 alloform. *J Am Chem Soc* 127:2075–2084.
37. Takano K, *et al.* (2006) Structure of amyloid β fragments in aqueous environments. *FEBS J* 273:150–158.
38. Ehrnhoefer DE, *et al.* (2008) EGCG redirects amyloidogenic polypeptides into unstructured, off-pathway oligomers. *Nat Struct Mol Biol* 15:558–566.
39. Lomakin A, Chung DS, Benedek GB, Kirschner DA, Teplow DB (1996) On the nucleation and growth of amyloid β-protein fibrils: Detection of nuclei and quantitation of rate constants. *Proc Natl Acad Sci USA* 93:1125–1129.
40. Condron MM, Monien BH, Bitan G (2008) Synthesis and purification of highly hydrophobic peptides derived from the C-terminus of amyloid β-protein. *Open Biotechnol J* 2:87–93.

Supporting Information

Fradinger *et al.* 10.1073/pnas.0807163105

SI Text

CTF Synthesis. CTFs were synthesized by Fmoc chemistry using automated Applied Biosystems 433A synthesizers. The synthesis scale was between 0.20 and 0.25 mmol. The coupling and deprotection cycles were extended from the manufacturer's recommended times, 30 and 10 min, to 60 and 30 min, respectively. Coupling cycles were performed by using 4 eq. of incoming amino acid, 4 eq. of *O*-benzotriazole-*N,N,N′,N′*-tetramethyluronium hexafluorophosphate, and 4 eq of *N,N*-diisopropylethyamine in *N*-methylpyrrolidone (NMP). Fmoc deprotection was done by using 20% piperidine in NMP. The ε-NH$_2$ group of Lys was protected by *tert*-butoxycarbonyl (BOC). Cleavage of the peptide from the resin and side-chain deprotection (where appropriate) were performed by using 10 ml of the following mixtures: (*i*) 9.5:0.5 trifluoroacetic acid (TFA):H$_2$O; (*ii*) 9.25:0.5:0.25 TFA:H$_2$O:ethanedithiol (EDT); (*iii*) 87.5:0.5:0.5:0.25 TFA:H$_2$O:thioanisole:EDT; or (*iv*) 9.5:0.25:0.25 TFA:EDT:triisopropylsilane. After filtration of the resin, several methods were used for isolation and purification of the crude peptides. For complete details, see ref. 1.

Cell Culture. Rat pheochromocytoma (PC-12) cells were maintained in F-12 nutrient mixture with Kaighn's modification (F-12K) with 15% heat-inactivated horse serum and 2.5% FBS at 37°C in an atmosphere of 5% CO$_2$. For cell viability assays, cells were plated in 96-well plates at a density of 30,000 cells per well in differentiation media (F-12K, 0.5% FBS, 100 μM nerve growth factor) and maintained for 48 h.

Primary mouse hippocampal cultures were generated from pregnant C57 black mice (E18). Embryos were removed from the uterus, and hippocampi were dissected and placed in sterile Hanks' buffered salt solution. Hippocampi were cut into 1-mm pieces, added to 1 ml of 0.05% trypsin and 0.001% DNase (Sigma), and incubated at 37°C for 15 min, agitating every 2–3 min to break apart clumps. Then, 3 ml of neurobasal media (Invitrogen) containing 10% FBS was added and the tissue was centrifuged for 5 min at 200 × *g* to gently pellet the cells. The cells were resuspended in neurobasal media by gentle trituration with a polished Pasteur pipette. Cells were plated at a density of 1–3×10^6 cells per milliliter on acid-treated, polyL-lysine (0.1 mg/ml)-coated 12-mm glass coverslips in 6-cm plastic culture dishes with 7 ml of growth media (neurobasal media, 2% B27 supplement, 500 μM glutamine, and 0.5% antibiotics). Cells were maintained for 2 weeks with changing half of the volume of the media twice weekly. After 2 weeks in culture, the cells had established synaptic connections and were ready for electrophysiological recordings.

Cell Viability Assays. To assess the biological activity of the CTFs themselves, peptide solutions were prepared by dissolving the CTFs in DMSO and diluting into F-12K media to yield concentrations of 1–200 μM. Aliquots of 10 μl were added to differentiated PC-12 cells to yield final concentrations of 0.1, 1, 5, 10, and 20 μM and incubated for 15 h. Negative controls included DMSO at the same concentration as in the peptide solutions and media alone. A positive control was 1 μM staurosporine for full kill. The staurosporine control was used to establish the dynamic range of the experiment and represented a 100% reduction in cell viability, based on which the percentage viability of all of the experimental conditions was calculated. The toxicity of all of the CTFs was studied at concentrations up to 20 μM because this is a concentration at which we observe a robust toxic effect for

Aβ42. We did not study higher CTF concentrations because inhibition assays using higher CTF concentrations demonstrated a rescue of Aβ42-induced toxicity, supporting that the CTFs remained nontoxic even at the highest concentration used. Cell viability was assessed qualitatively by visual observation and quantitatively by the CellTiter 96 Non-Radioactive Cell Proliferation Assay (Promega). Briefly, 15 μl of dye solution was incubated with the cells for 3 h. Then 100 μl of solubilization/stop solution was added and the plates were incubated overnight in the dark to ensure complete solubilization. Plates were read by using a Synergy HT microplate reader (BioTek), and the absorbance at 570 nm (formazan product) minus the absorbance at 630 nm (background) was recorded. Corrected absorbance was used to calculate the percent cell viability from the experimental change ($A_{\mathrm{media}} - A_{\mathrm{experimental}}$) over the dynamic range ($A_{\mathrm{media}} - A_{\mathrm{staurosporine}}$). At least three independent experiments with six replicates ($n \geq 18$) were carried out, and the results were averaged.

To test for inhibitory effect the CTFs on Aβ42-induced toxicity, solutions of Aβ42 and CTF at a ratio of 1:10 were prepared. Control experiments with Aβ42 alone showed that 5 μM Aβ42 caused a robust ($\approx$40%) reduction in cell viability. CTFs were dissolved in DMSO and diluted with Aβ42 solutions. The mixtures were subjected to a brief centrifugation to remove preformed aggregates, and then aliquots of 10 μl were immediately added to cells to yield final concentrations of 50 μM CTF and 5 μM Aβ42. Although the solutions were all clear to the eye, it is possible that some aggregation occurred upon dilution in the medium. As a result, it is possible that the actual soluble CTF concentration was lower than the nominal concentration. Cell viability was determined by the MTT assay as described above. At least three independent experiments with six replicates ($n \geq 18$) were carried out, and results were averaged. CTFs that showed strong inhibition of Aβ42-induced toxicity were studied further to determine their dose-dependent activity.

Dose-dependence MTT experiments with Aβ(31–42) and Aβ(39–42) were conducted as described above with final Aβ42:CTF ratios of 1:0, 1:1, 1:2, 1:5, and 1:10 for both CTFs and 1:20, 1:15 for Aβ(39–42) only. Three independent experiments with five to six replicates ($n \geq 15$) were carried out, and results were averaged.

In addition, dose dependence LDH release experiments were performed using the CytoTox-ONE Homogenous Membrane Integrity Assay (Promega). Control experiments with Aβ42 alone identified a concentration of 10 μM that yielded robust cell death. Aβ42 was mixed with either Aβ(31–42) or Aβ(39–42) at ratios from 1:1 to 1:10. Because DMSO somewhat permeabilizes cell membranes and causes high background in this assay, all peptides were dissolved initially in 60 mM NaOH and then diluted into media. [In separate MTT experiments, the toxicity of Aβ solubilized by either DMSO or 60 mM NaOH was compared. The data showed slight ($<$10%) increase in the toxicity of DMSO-solubilized Aβ42 relative to peptide that was solubilized in 60 mM NaOH (P. Maiti and G.B., unpublished results).] A 10-μl aliquot of each mixture was added to the cells to yield final concentrations of 10–50 μM [Aβ(31–42)] or 10–100 μM [Aβ(39–42)] and 10 μM Aβ42. Cells were incubated with peptide mixtures for 48 h and then assayed for cell death. Briefly, cells were incubated at room temperature for 20 min, then 100 μl of dye solution were added and incubated for 10 min at room temperature. Fifty microliters of stop solution were added, and the plates were read at an excitation wavelength of

560 nm and emission wavelength of 590 nm. Three individual experiments of five to six replicates were carried out ($n \geq 15$), and the results were averaged.

Electrophysiological Studies. On the day of the experiment, a coverslip of hippocampal culture was transferred to the recording chamber (Warner RC-25F) of an inverted microscope (DIAPHOT 300; Nikon), and cells were perfused with an "extracellular solution" (130 mM NaCl/5.4 mM KCl/1.8 mM $CaCl_2$/0.8 mM $MgCl_2$/10 mM D-glucose/10 mM Hepes/0.02 mM bicuculline methiodide/0.1 mM tetrodotoxin, pH 7.4). Spontaneous mEPSCs were measured by using whole-cell recordings. Glass microelectrodes filled with a solution composed of 105 mM CsCl, 2.5 mM $MgCl_2$, 10 mM EGTA, 40 mM Hepes, 5 mM D-glucose, 4 mM Mg-ATP, and 0.5 mM Na-GTP (pH 7.2). The mEPSCs were recorded at a holding potential of -70 mV in cultured neurons with a membrane seal of 3–5 MΩ by using a patch-clamp amplifier model Axopatch 200A (Axon Instruments) and digitized by using a Digidata 1322A Interface (Axon Instruments). Signals were filtered at 2 kHz and sampled at 10 kHz. Continuous recording and analysis of mEPSCs were performed with Minianalysis software (Synaptosoft). Cells were perfused at a flow rate of 0.4–0.5 ml/min with peptide samples of 3 μM Aβ42, 1:1 or 1:10 Aβ42:CTF, or vehicle control (extracellular solution with DMSO). To calculate mEPSC amplitude and frequency, events were analyzed for 1 min before and every 5 min during the application of peptide samples. Data are presented as mean $\pm$ SE. Statistical significance was assessed by using Student's t test.

Dynamic Light Scattering (DLS). Aβ42:CTF mixtures containing 30 μM nominal concentration each of Aβ42 and Aβ(31–42) or Aβ(39–42) were studied by using an in-house-built system with a He-Ne laser (wavelength 633 nm, power 50 mW; Coherent) as a light source and an arrangement of collection optics that is optimized for maximal sensitivity. Light scattered at 90° was collected by using image transfer optics and detected by an avalanche photodiode built into a 256-channel correlator (Precision Detectors). The size distribution of scattering particles was reconstructed from the scattered light correlation function by using PrecisionDeconvolve deconvolution software (Precision Detectors) based on the regularization method by Tikhonov and Arsenin (2).

Two-hundred-microliter samples were lyophilized, stored at -20°C, and then reconstituted in 200 μl of water. The solutions were sonicated for 60 s and filtrated through a syringe filter (20-nm pore size; Whatman) before DLS measurements. The actual concentration was measured by amino acid analysis (AAA). Two replicates with similar concentrations each of Aβ42 and CTF were measured for each condition.

Photo-Induced Cross-Linking of Unmodified Proteins (PICUP). CTFs were dissolved in 60 mM NaOH and diluted into 10 mM sodium phosphate (pH 7.4; 1:10 vol/vol) to yield a nominal concentration of 200 μM. Preformed aggregates were removed by filtration through a 20-nm pore size filter. Low-molecular-weight (LMW) Aβ42 was prepared by ultrafiltration as described previously (3). The actual concentration of each solution was determined *post facto* by AAA. Each CTF was mixed with LMW Aβ42 at an $\approx$1:1 concentration ratio, and the mixtures were immediately sub-

jected to PICUP as described previously (4, 5). Only experiments yielding similar ($\pm$10%) concentrations were each of Aβ42 and CTF were taken into account. All of the CTFs contain only amino acid residues with low reactivity in PICUP chemistry (5); therefore, cross-linking occurred only among Aβ42 molecules. The cross-linked peptide mixtures were analyzed by SDS/PAGE, and Aβ42 hexamer abundance was quantified by densitometric analysis using One-Dscan (Scanalytic) as described previously (6, 7). Hexamer intensity was normalized to the intensity of the entire lane for each CTF.

***Ab Initio* Discrete Molecular Dynamics (DMD).** In DMD, all interparticle potentials are replaced by a square-well or a combination of square-well potentials. The resulting dynamics is driven by collisions between particles, which are otherwise moving along straight lines with constant velocities. The Berendsen thermostat algorithm (8) is periodically applied to keep the temperature of the system constant. We use a four-bead protein model in which the backbone is modeled by three atoms/beads (corresponding to the amide N, the α-carbon C_α, and the carbonyl C' groups), and the side chain is represented by one bead, C_β (with exception of G, which has no side-chain bead) (9). An effective backbone hydrogen bond is introduced between the nitrogen atom N_i of the ith amino acid and the carbon atom C'_j of the jth amino acid (9). Effective hydropathic interactions among side-chain atoms are introduced to mimic the solvent effects (10). The relative strength of hydropathic interactions between pairs of side-chain beads is based on the Kyte–Doolittle hydropathy scale (11). In our model, the hydrophobic amino acids are A, C, F, L, M, I, and V, and hydrophilic amino acids are D, E, H, K, N, Q, and R. The side chains of the remaining amino acids G, P, S, T, W, and Y interact only through steric repulsion. All model parameters are set to the same values as used in the previous study (10). We set the potential energy of the hydrogen bond, E_{HB}, to unit energy ($E_{HB} = 1$) and the maximal absolute value of the potential energy of the hydropathic interactions $E_{HP} = 0.3$, such that the potential energy of two interacting Ile side chain beads is -0.3. Using the unit of temperature E_{HB}/k_B where k_B is Boltzmann's constant, we use $T = 0.15$ as a reasonable estimate of physiological temperatures.

Contact Maps. By definition, two beads are in contact if they are at a distance equal to or smaller than 7.5 Å. A contact map is a matrix in which the value of each (i,j) element is equal to an average number of contacts between amino acids i and j. We consider two types of contact maps: intramolecular and intermolecular contact maps. If amino acids i and j belong to the same peptide, the corresponding contacts contribute to the intramolecular contact map, otherwise, to the intermolecular contact map. The contact map of each assembly is normalized by the number of contributing peptide molecules. Because in our model each amino acid is represented by up to four beads, the maximal number of intramolecular contacts between residues i and j is $4 \times 4 = 16$. The maximal number of intermolecular contacts between residues i and j can be larger than 16 because amino acid i of one molecule can be surrounded by several amino acids j from multiple molecules. All contact maps were first calculated separately for each heterooligomer and then averaged over all assemblies under consideration.

1. Condron MM, Monien BH, Bitan G (2008) Synthesis and purification of highly hydrophobic peptides derived from the C-terminus of amyloid β-protein. *Open Biotechnol J* 2:87–93.
2. Tikhonov AN, Arsenin VY (1977) *Solution of Ill-Posed Problems* (Halsted, Washington, DC).
3. Bitan G, Teplow DB (2005) Preparation of aggregate-free, low molecular weight amyloid-β for assembly and toxicity assays. *Methods Mol Biol* 299:3–9.
4. Bitan G, Teplow DB (2004) Rapid photochemical cross-linking—A new tool for studies of metastable, amyloidogenic protein assemblies. *Acc Chem Res* 37:357–364.
5. Bitan G (2006) Structural study of metastable amyloidogenic protein oligomers by photo-induced cross-linking of unmodified proteins. *Methods Enzymol* 413:217–236.
6. Bitan G, *et al.* (2003) Amyloid β-protein (Aβ) assembly: Aβ40 and Aβ42 oligomerize through distinct pathways. *Proc Natl Acad Sci USA* 100:330–335.

7. Bitan G, Lomakin A, Teplow DB (2001) Amyloid β-protein oligomerization: Prenucleation interactions revealed by photo-induced cross-linking of unmodified proteins. *J Biol Chem* 276:35176–35184.

8. Berendsen HJC, Postma JPM, van Gunsteren WF, DiNola A, Haak JR (1984) Molecular dynamics with coupling to an external bath. *J Chem Phys* 8:3684–3690.

9. Ding F, Borreguero JM, Buldyrey SV, Stanley HE, Dokholyan NV (2003) Mechanism for the α-helix to β-hairpin transition. *Proteins* 53:220–228.

10. Urbanc B, *et al.* (2004) *In silico* study of amyloid β-protein folding and oligomerization. *Proc Natl Acad Sci USA* 101:17345–17350.

11. Kyte J, Doolittle RF (1982) A simple method for displaying the hydropathic character of a protein. *J Mol Biol* 157:105–132.
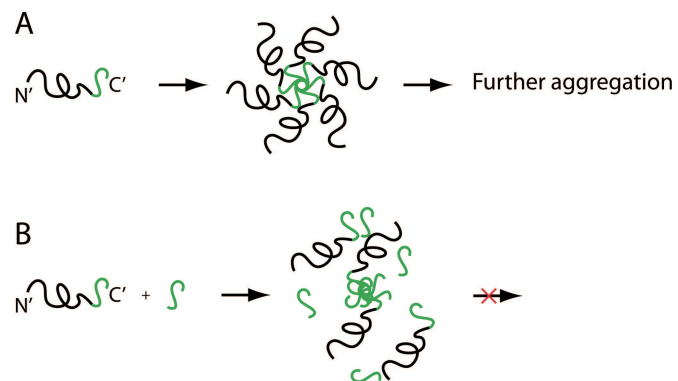
Fig. S1. Schematic representation of Aβ42 CTFs as inhibitors of full-length Aβ42 oligomerization. (*A*) The C termini (green) of several Aβ42 molecules are hypothesized to form the hydrophobic core of oligomers. (*B*) CTFs derived from the C terminus of Aβ42 coassemble with the C terminus of the full-length peptide, leading to disruption of oligomerization.
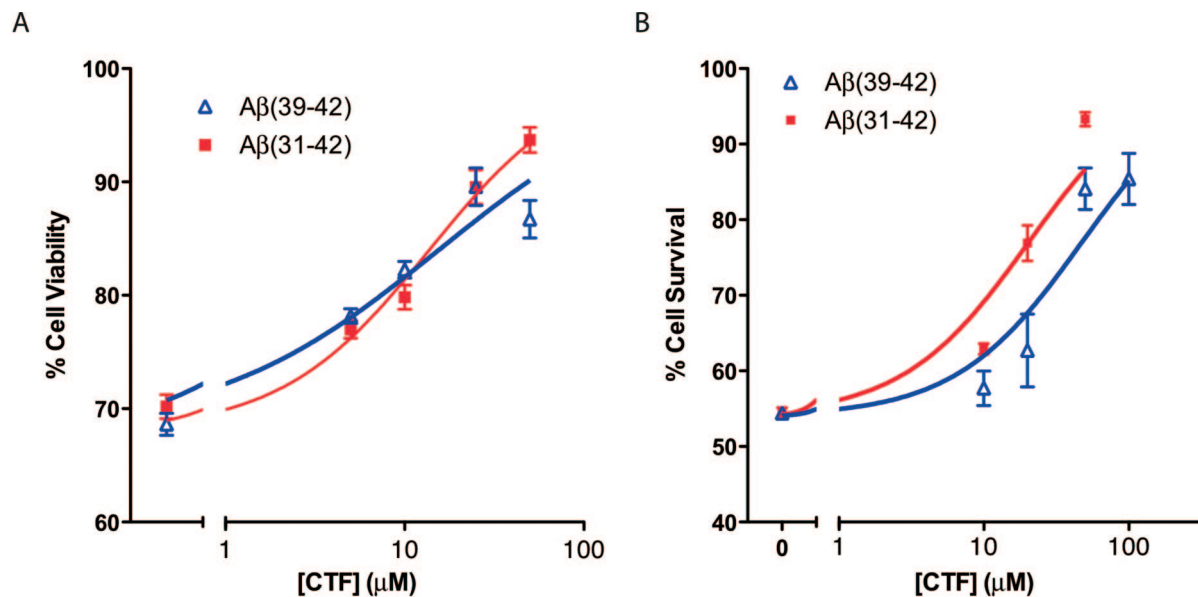
Fig. S2. Dose-dependent inhibitory activity of Aβ(31–42) and Aβ(39–42). (*A*) Cell viability determined by the MTT assay in differentiated PC-12 cells in the presence of 5 μM Aβ42 and Aβ42:CTF concentration ratios ranging from 1:0 to 1:10. The data were normalized to full-kill and media controls and reported as mean $\pm$ SD (n = 15–18). (*B*) Cell death determined by the LDH release assay in differentiated PC-12 cells in the presence of 10 μM Aβ42 and Aβ42:CTF concentration ratios ranging from 1:0 to 1:5 for Aβ(31–42) and 1:10 for Aβ(39–42). The data were normalized to full-kill and media controls and are reported as mean $\pm$ SD (n = 18–24).
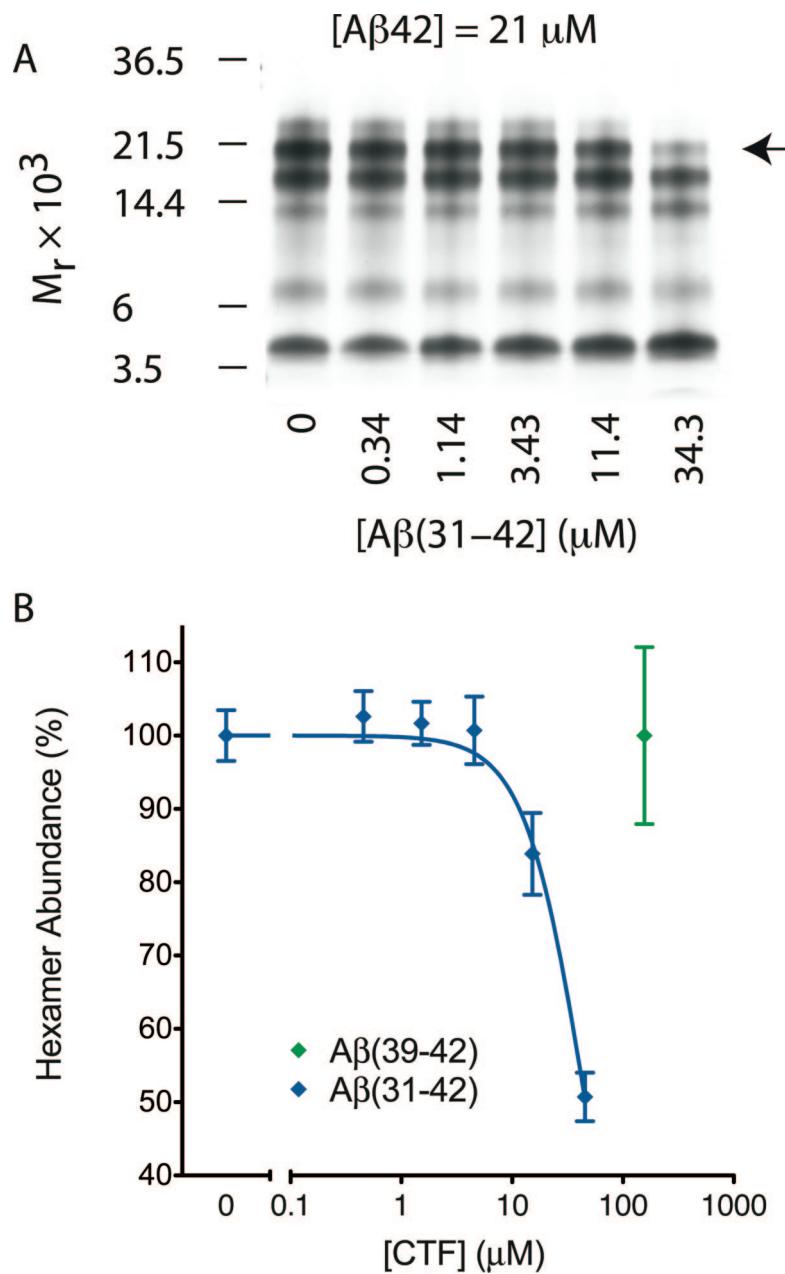
Fig. S3. PICUP analysis. (*A*) A representative experiment is shown. LMW Aβ42 was mixed with increasing concentrations of Aβ(31–42) and photo-cross-linked immediately. The mixtures were fractionated by SDS/PAGE and silver-stained. Positions of molecular weight markers are shown on the left. Aβ(31–42) concentration is given at the bottom of each lane. (*B*) Densitometric analysis of hexamer abundance normalized to the entire lane in experiments similar to those shown in *A* for Aβ(31–42). Data measured at a single concentration (155 ± 10 μM) is shown for Aβ(39–42). The data are presented as mean ± SE measured in three independent experiments.
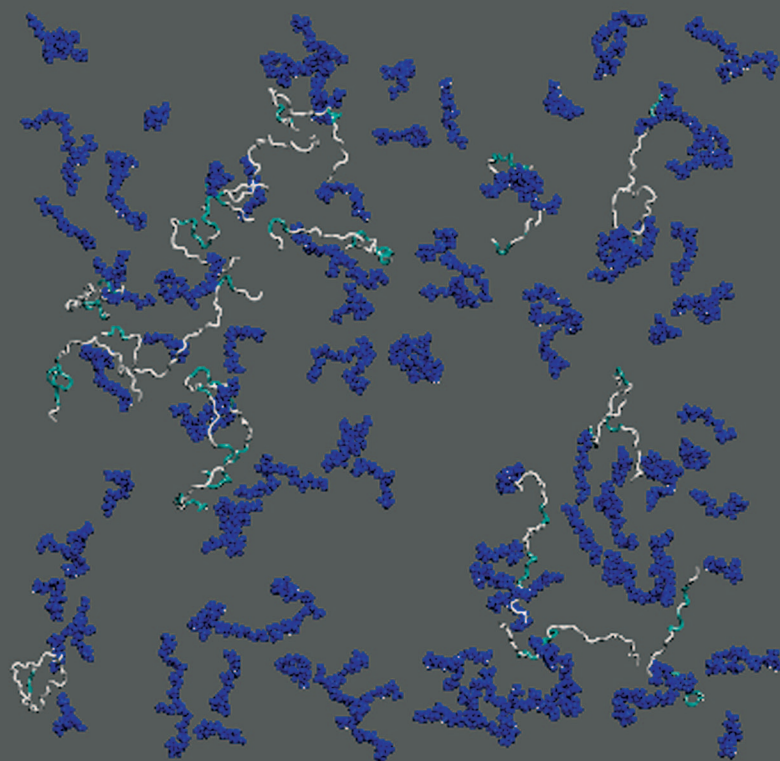
Movie S1.   Simulation of the interaction between 16 Aβ42 molecules and 128 Aβ(31–42) molecules between 0 and 10-million simulation steps.

Movie S1 (GIF)